ARTICLE

Quantitative Investigation of the Photodegradation of Polyethylene Terephthalate Film by Friction Force Microscopy, Contact-Angle Goniometry, and X-ray Photoelectron Spectroscopy

Claire R. Hurley and Graham J. Leggett*

Department of Chemistry, University of Sheffield, Brook Hill, Sheffield S3 7HF, United Kingdom

ABSTRACT Studies of the UV-induced photodegradation of poly(ethylene terephthalate) (PET) have been carried out using contact-angle goniometry, X-ray photoelectron spectroscopy (XPS), and friction force microscopy (FFM). The advancing contact angle of water, θ, decreased following exposure of free-standing PET films to UV light. Measurements of surface friction by FFM showed that the coefficient of friction μ increased as the degradation proceeded, reaching a limiting value after ca 200 min, in agreement with the contact angle data. Using a modified form of the Cassie equation, a quantitative analysis of the extent of modification could be carried out. There was a very close correlation between the coefficient of friction determined by FFM and the value of cos θ. XPS provided more detailed information on surface bonding that also correlated closely with the FFM data. Although FFM provides quantitative data on surface modification with nanometer-scale spatial resolution, it does not provide detailed structural information such as is provided by XPS. The oxygen content at the surface was found to increase as photo-generated radicals within the PET reacted with atmospheric oxygen. Increases in both ester and carbonyl contributions within XPS data accompanied this increase. It was concluded that the photodegradation process follows mainly Norrish type I reaction pathways, following previous work by Fechine et al and Grosstête et al.

KEYWORDS: polymer surface • friction force microscopy • X-ray photoelectron spectroscopy • poly(ethylene terephthalate) • photodegradation • contact angle goniometry

INTRODUCTION

The quantitative investigation of surface structure and chemical composition at the nanometer scale remains a significant challenge in surface analysis. Although substantial advances have been made in recent years in the analysis of surfaces by secondary ion mass spectrometry (SIMS) at high resolution, characterization at a resolution of tens of nanometers remains difficult, and other conventional surface analysis techniques yield data with substantially lower resolution. Friction force microscopy (FFM) has emerged as a powerful tool for the investigation of nanometer scale tribological phenomena (1−6), and its capacity for qualitative investigation of surfaces is well-established. There has been a great deal of interest in using FFM to study molecular tribological phenomena, and it has been used to study a wide range of molecular interfaces, including self-assembled monolayers of alkylsiloxanes (7−10), alkanethiols (11−17), alkoxy compounds (18), alkylphosphonic acids (19, 20), and polymers (21, 22). Importantly, however, it is becoming clear that through comparatively simple analyses of FFM data, it is possible to obtain information of surface chemical composition that is quantitative, at high spatial resolution. For example, FFM has been used to quantify rates of photopatterning processes at a resolution of a few tens of nanometers (23). Such data are not accessible by any other analytical technique. In previous studies of surface composition by FFM, attention has largely focused on the analysis of well-defined monolayer systems. The goal of the present work is to extend such methodologies to polymer systems, because polymer surfaces constitute an important class of materials and because they remain difficult to characterize at high spatial resolution by conventional tools. In particular, the photodegradation of poly(ethylene terephthalate) (PET) has been investigated by FFM, and the data compared with those obtained by analysis of measurements made by contact angle and X-ray photoelectron spectroscopy (XPS).

Photochemical processes are a major cause of degradation in polymeric materials (24 –26), and thus present an important class of problem on which to test the utility of quantitative data obtained from FFM measurements. Photooxidation under controlled conditions is a useful means of simulating the aging process (26) and for exploring the impact of processing steps during manufacturing, such as drawing (27, 28) and the incorporation of additives (29, 30). Photodegradation also causes polymer breakdown and may contribute to waste reduction (31, 32). Surface modification by photodegradation (33, 34) is used to aid the attachment

* Corresponding author. E-mail: Graham.Leggett@shef.ac.uk.
Received for review April 9, 2009 and accepted July 14, 2009

DOI: 10.1021/am900250q

Published on Web 07/28/2009

Scheme 1. Norrish Type I and II Reactions of PET

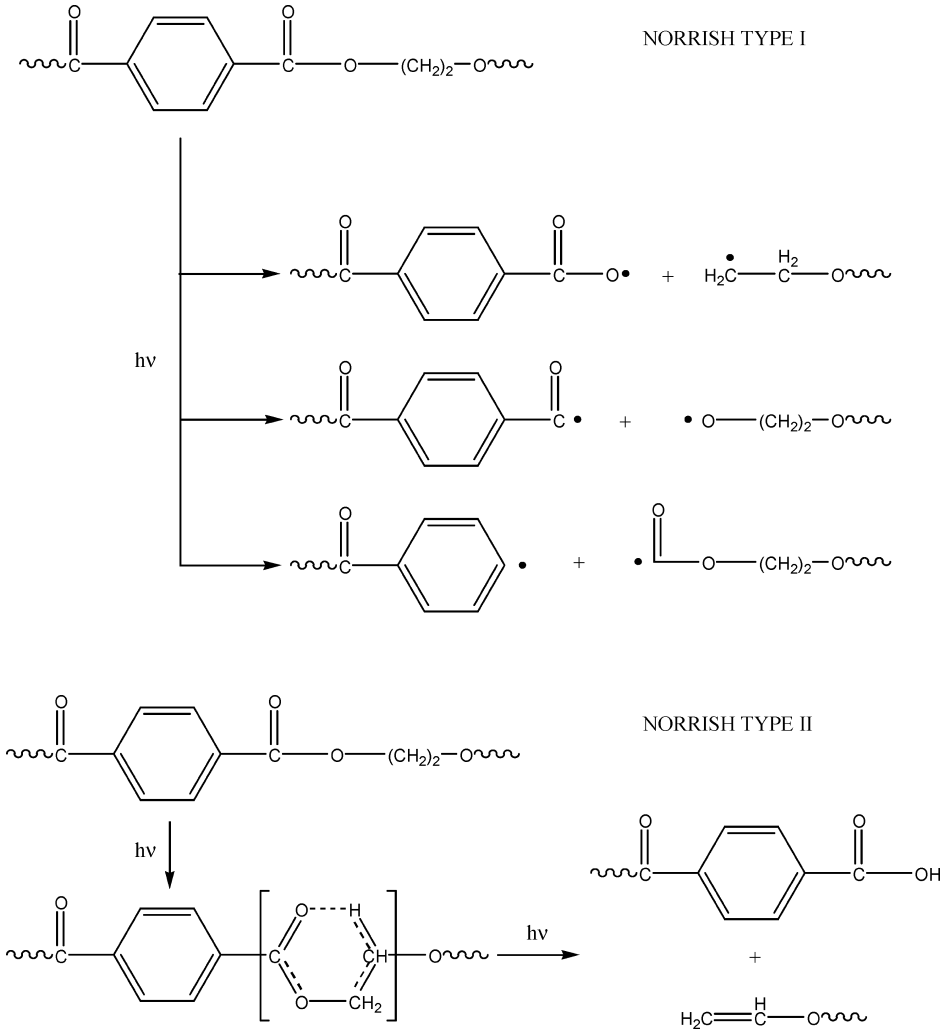

of enzymes and antibodies to surfaces in bioassays. To understand such phenomena, it is valuable to have the ability to make quantitative measurements of surface structure and composition with high spatial resolution.

There has been a substantial amount of work on the photodegradation of PET, although the mechanisms are not fully understood (35). A wide range of wavelengths have been investigated, from the deep UV (36−38) to the near UV (24−26, 29−31, 39). The main degradation process during photo-oxidation of PET is known to be chain scission leading to a decrease in molecular weight of the polymer and the generation of carboxyl end groups, particularly at the surface. The activated ketones can fragment via two pathways: the Norrish Type I and II mechanisms (40) (Scheme 1). The Norrish Type I reaction involves the formation of radicals around the ester linkage and termination of the polymer chains. The Norrish Type II reaction occurs via intramolecular abstraction of a γ-hydrogen through a cyclic intermediate and results in the termination of polymer chains ending in carboxylic acids and alkenes (39). In addition the evolution of volatile products such as carbon monoxide and carbon dioxide is observed. Day and Wiles have proposed a Norrish Type II pathway arguing that the carboxyl end groups are not generated by reaction with oxygen but via a cyclic intermediate (40). In contrast, Fechine et al. have reported a depth-dependence in the photo-degradation process (29) and have proposed an alternative mechanism (Scheme 2) based on Norrish Type I reactions that proceed via a radical species to produce mono or hydroxy terephthalates, carboxyl end groupsm and aldehydes. This mechanism proceeds via the main radical discussed by Grossetête et al., who indicated the possibility of further reaction from the aldehyde to another carboxylic acid (38).

In the present study, the photodegradation processes in a free-standing film of polyethylene terephthalate (Melinex OD) have been investigated following exposure to light with a wavelength of 254 nm. Evidence has been provided that FFM may be used to derive quantitative information on the effects of photodegradation on polymer structure and composition. On the basis of XPS data, a mechanism for PET photodegradation is proposed that is very similar to that of Fechine et al.

EXPERIMENTAL SECTION

Melinex OD Film (thickness 125 μm) was obtained from DuPont Teijin Films. Prior to exposure, 1 cm^2 samples were sonicated for 5 min in diethyl ether and dried under a stream of nitrogen to remove any particulates.

Scheme 2. Proposed Mechanism for the Photo-oxidation of PET; This Mechanism Proceeds via Norrish Type I Reactions

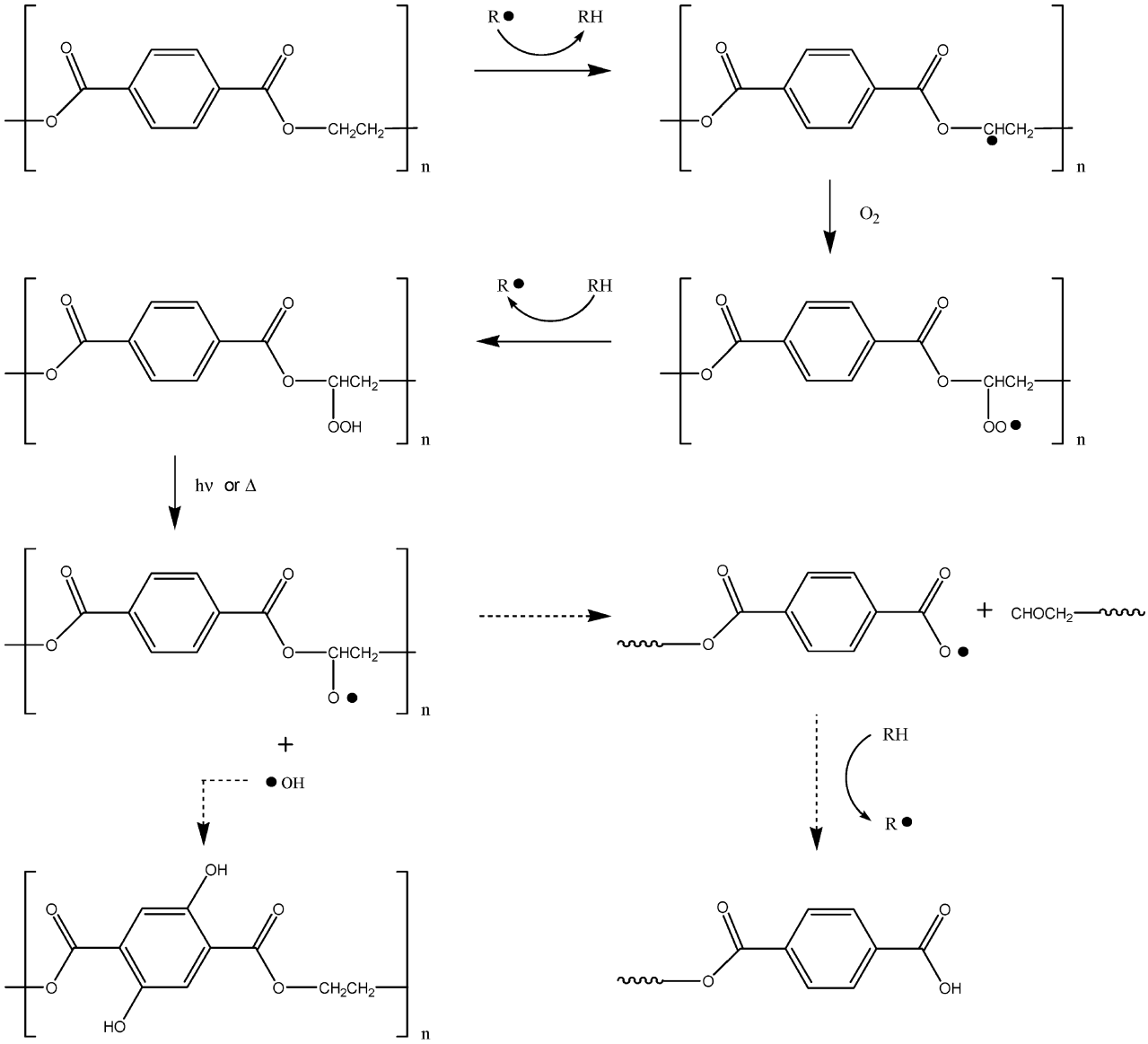

Photo-oxidation was carried out using a UV lamp (model R-52G) emitting at 254 nm with a power of ~1 mW cm^{-2} measured using a power meter. The lamp was switched on and left to equilibrate for 10 min prior to sample treatment. PET films were treated at a constant distance of 3 cm. The length of the exposure, performed under ambient conditions, ranged from 0 to 6 h to allow complete irradiation of the sample surface. Samples were analyzed within 40 min of UV treatment with the exception of samples submitted for XPS analysis, which were stored in low light conditions overnight.

Sessile drop water contact angles were measured using a Rame-Hart 100−00 goniometer. A 2μL droplet was released from a syringe suspended above the sample stage. The sample was raised until it contacted the droplet whereupon the stage was retracted slowly until the drop broke free of the meniscus formed with the syringe. The droplet was then allowed to stabilize for 1 min before the advancing contact angle was measured. A minimum of four contact angles was obtained on different samples for each exposure time. These experiments were repeated with surfaces immersed in ethanol for 30 min immediately after exposure in order to remove low-molecular-weight material at the surface.

FFM measurements were performed on a Digital Instruments Nanoscope IIIa Multimode Atomic Force Microscope operating in contact mode. The tips were silicon nitride Nanoprobes (Digital Instruments, Cambridge, UK) with nominal force constants of 0.06 N m^{-1}. To acquire quantitative data on the surface using FFM it was necessary to calibrate the Nanoscope. This calibration of normal forces involved two steps. First, the photodetector sensitivity was calibrated by measuring a force curve for the cantilever in contact with a stiff sample (mica). Relative to the cantilever, the stiffness of mica is sufficiently large that it may be assumed that all deflection during the force measurement will be in the lever. Under these circumstances, the photodetector sensitivity is the gradient of a plot of photodetector signal versus displacement while measuring repulsive forces. The spring constants of the levers were determined from their thermal spectra using a routine implemented within the microscope software (Digital Instruments PicoForce software) and based on the method of Hutter and Bechhoefer (41). This

approximates the cantilever as a harmonic oscillator, the motion of which is driven by thermal noise. Applying the equipartition theorem, Hutter and Bechhoefer derived a relationship between the spring constant and the power spectrum of the cantilever response. Experimentally, the laser spot was focused on the apex of the cantilever, and the thermal fluctuations of the cantilever were measured and used to derive the power spectrum. Prior to any measurements the applied load was minimized recording the set point value of zero load. This was done by retracting the tip, allowing it to lose contact with the surface and extending it until it snapped back into contact. Quoted loads are the products of the spring constants; photodetector sensitivities and deflection set points.

To minimize uncertainty due to the many parameters influencing the tip-sample interaction, we used the same probe throughout whole experiments. Trace-retrace subtraction of data from friction loops enabled elimination of topographical effects from the data, giving a resultant signal equivalent to twice the frictional force (1, 2). Experiments were performed under ethanol using a liquid cell fitted with a silicone O-ring to enable the use of Amontons' law to model these data (21). The AFM was first setup to image the surface; simultaneous comparison of friction images with topographical imaging ensured the tip was still in contact. Friction loops were acquired from an initial set point of ~2.5 V, and the load was then reduced incrementally in steps of 0.2 V until the tip pulled free of the surface. Areas of 5 μm^2 were scanned with 256 scan lines at a frequency of 1 Hz to minimize sample damage. Measurements were taken at three positions on three sample surfaces for each exposure time, and from these an average friction coefficient was obtained.

XPS measurements were taken on a Kratos Axis Ultra X-ray photoelectron spectrometer. Samples were prepared 12 h in advance and stored in low light conditions overnight. Immediately prior to XPS analysis samples were maintained under a vacuum of 1×10^{-8} mbar for approximately 2 h. A minimum of three XPS spectra was obtained on different sample runs for each exposure time. Analysis was carried out using CasaXPS software (Casa, http://www.casaxps.com, UK). Survey and narrow scan spectra of C1s and O1s peaks were obtained. Peaks were fitted using combinations of Gaussian (30%) and Lorentzian (70%) curves against a linear background. The FWHM of all components was constrained to be equal to that of the aliphatic carbon, but all other parameters were left free to vary during fitting, optimizing parameters taken from a PET table of standard spectra (42). These experiments were repeated with surfaces immersed in ethanol for 30 min immediately proceeding exposure in order to remove low-molecular-weight material at the surfaces.

To test for hydroxyl group incorporation into UV-modified PET samples (see Scheme 2), they were attached to glass slides using an adhesive carbon tab. The slides were then mounted at a 45° angle in an enclosed sample tube containing 100 μL of trifluoro acetic anhydride (TFAA). Samples were left in a saturated, ambient TFAA environment for 1.5 h. The films were then washed with ethanol and dried in a low stream of nitrogen gas to remove any excess reagent.

RESULTS AND DISCUSSION

Contact-Angle Measurement. The effect of UV exposure was first monitored by contact angle goniometry (Figure 1). The contact angle was initially 76 ± 2°, in agreement with previously published values, and decreased following UV exposure. This behavior was consistent with the expected increase in surface oxygen content brought about by irradiation of the surface, which photosensitizes the polymer and causes it to react with atmospheric oxygen.

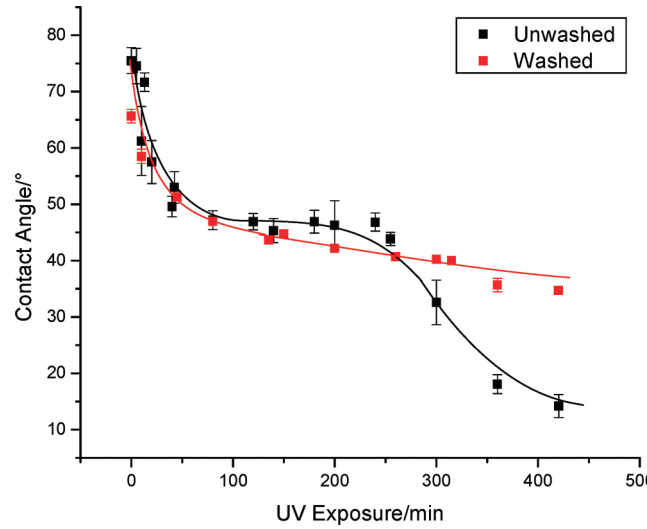

FIGURE 1. Reduction in the contact angle as PET is exposed to 254 nm UV light over 7 h.

This increase in overall surface oxygen results in increasing dipole−dipole interactions and hydrogen bonding with the water droplet, and hence the surface becomes more hydrophilic (36, 43).

Initially, the rate of decrease in the contact angle was high, but it declined, and the rate of change began to approach zero after 100 min, when the contact angle was 47°. However, as the exposure was increased still further, the contact angle again began to fall and eventually reached a minimum of 14 ± 2°, following exposure for 7 h. A sigmoidal curve was fitted to the data, suggesting a two-step process.

Previous studies have reported that the contact angle of PET falls from ca. 75° to ca. 40° following UV exposure. Arefi-Khonsari et al. studied PET surfaces after both laser and plasma treatments. After plasma treatment for 5 s, the contact angle had stabilized and was reduced from 77 ± 3° to 38°, whereas after laser treatment, the wettability was enhanced to different degrees depending on the laser fluence, a lower fluence resulting in a higher surface wettability (37). The lowest contact angle achieved in this case was also 38°. Similar results have been obtained by other authors (36). These findings were consistent with the behavior observed here over the first 100 min. However, here a further reduction was also observed in the contact angle after long exposures.

To test whether this could be connected with the formation of low-molecular-weight material at the sample surface, the experiments were repeated and each sample was immersed in ethanol for 30 min prior to contact-angle measurement to remove any surface debris. Following rinsing in this fashion, the behavior was significantly altered: the second period of declining contact angle was absent and the contact angle did not change significantly after ca. 200 min. These data suggest that the second period of falling contact angles measured for the unwashed samples is due to the formation at the surface of low-molecular-weight hydrophilic material that is removed by washing in ethanol. Grossetête reported the removal of photo-oxidized material from the

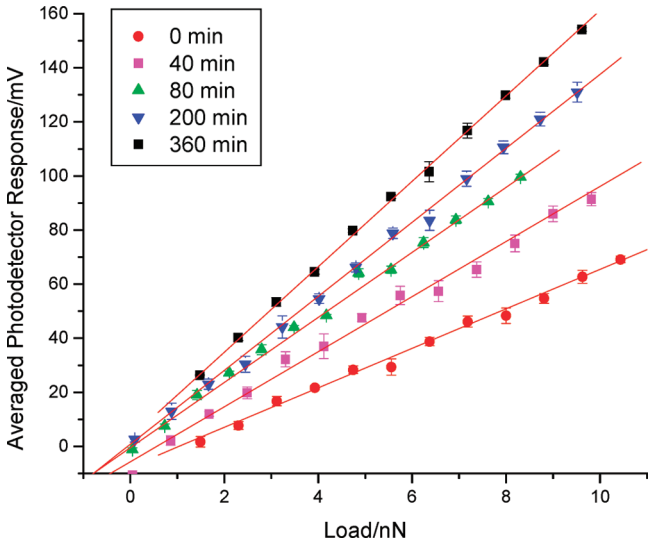

FIGURE 2. Friction-load plots after a 360 min UV exposure at 254 nm.

PET surface following 24 h immersion in methanol. Analysis of the wash showed evidence of molecular terephthalic acid, and that some of the low-molecular-weight material was the substituted terephthalate (38).

Friction Force Microscopy. FFM was performed on PET exposed to 254 nm UV light for 0, 40, 80, 135, 200, 260, and 360 min. These measurements were performed under ethanol because previous studies have shown that in this medium, FFM data may be analyzed using Amontons' law (ie. a linear relationship is typically observed between the friction force and the applied load) (21). Because of this, the experiment is also equivalent to the contact angle experiment conducted following washing of the sample.

Typical friction-load plots obtained on PET at a selection of representative exposure times are shown in Figure 2. In all cases, the photodetector response (which is proportional to the friction force) increased linearly as the load was increased, in accordance with the predictions of Amontons' law. Straight lines could be fitted to the data by linear regression with a regression coefficient of at least 0.998 in all cases. Within experimental error, the lines were found to pass through the origin (data for 0, 40, and 80 min exposure have been shifted vertically to aid clarity). A gradual increase was observed in the magnitude of the gradient as the exposure time increased. Friction coefficients, μ, were determined from the gradients of the friction-load plots, and normalized to the largest value measured. These are shown as a function of the UV exposure time in Figure 3. The normalized coefficient of friction increased from 0.47 ± 0.02 to 1.00 ± 0.03 over 360 min. The friction coefficient reached a limiting value after ca. 200 min, in agreement with the contact angle measurements for the washed PET. The data in Figure 3 were fitted with an exponential function.

In the present case, a silicon nitride probe was used, the outer surface of which consisted of silicon dioxide, a polar material. As the surface became more hydrophilic, it would be expected that the strength of the non-covalent attractive

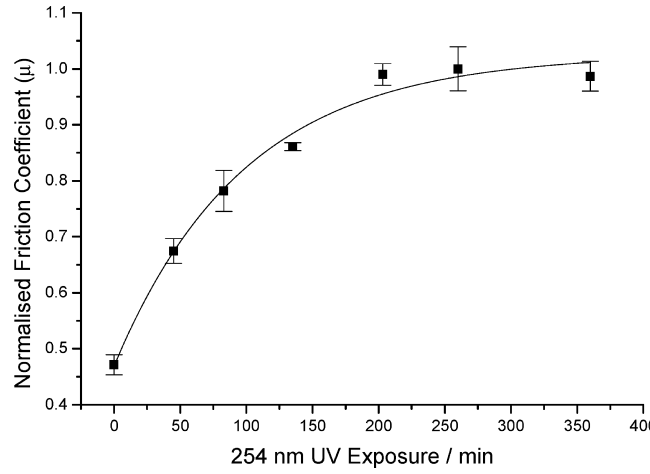

FIGURE 3. Observed increase in normalized friction coefficients as PET is exposed to 254 nm UV light over 360 min.

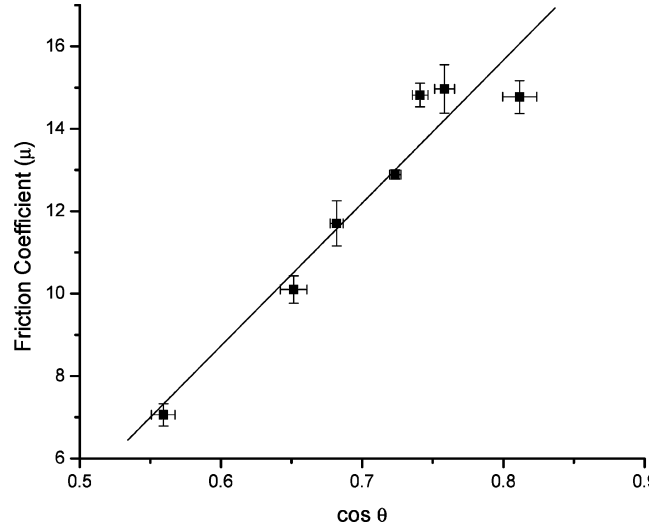

FIGURE 4. Relationship between the coefficient of friction (μ) and the cosine of the advancing water contact angle (cos θ).

forces acting at the tip-sample contact would increase (16, 43, 44). As a consequence, more work must be done shearing intermolecular interactions as the tip slides across the surface, leading to a higher rate of energy dissipation and hence a stronger frictional interaction. The data in Figure 3 reflect this, with the increase in the normalized value of the coefficient of friction being clearly correlated with the increase in wettability shown in Figure 1.

The extent of agreement between data obtained on the macroscopic and nanometer scales is demonstrated explicitly in Figure 4, which shows the variation in the friction coefficient with cos θ. A linear relationship was observed, suggesting that the data were correlated. Cos θ is approximately proportional to the interfacial free energy, and determines the work of adhesion at the tip-polymer contact. A linear relationship was previously reported between cos θ and μ in studies of mixed self-assembled monolayers (16, 45, 46); the present work supports these findings and shows that similar correlations exist for treated photodegraded PET surfaces. As the photo-degradation continues the surface is seen to become more hydrophilic and there-

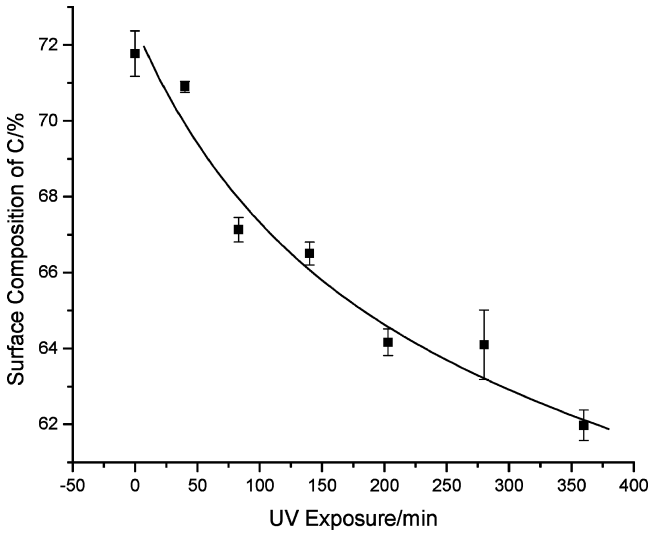

FIGURE 5. Decrease in the surface composition of carbon over the exposure to 254 nm UV light.

fore loses some of its ability to dissipate energy; this change occurs in a quantifiable manner.

The data in Figure 1 suggest that low-molecular-weight material may be created during the UV degradation of PET. In previous AFM studies of the plasma treatment of PET (43), it was reported that substantial changes in surface morphology occurred, that were attributed to preferential etching of the amorphous fraction of the polymer yielded. In the present study; however, AFM topographical images exhibited only small changes to surface morphology resulting from UV exposure, suggesting that the rate of removal of material was slow and indicating that changes in surface friction were attributable to modification of surface chemical structure rather than, for example, a change in the amorphous/crystalline ratio.

X-ray Photoelectron Spectroscopy. XPS analysis was used to determine the change in surface composition following exposure to UV light. A series of survey scans were taken over the range of exposure times (not shown). The samples exhibited only peaks due to oxygen and carbon. The surface composition was determined, and the results are shown, as at % carbon, in Figure 5. The carbon content was found to decrease from 71.8 ± 0.7% to 62.2 ± 0.9% over 6 h. The decrease was attributed to reaction between atmospheric oxygen and the radical species formed within the PET by UV exposure. Additionally, it is likely there was a loss of volatile species such as CO and CO_2. There was a corresponding increase in the percentage composition of oxygen in agreement with the work of Kikuchi et al. The compositions of the washed and unwashed samples were found to be indistinguishable (including washed and unwashed unirradiated samples). This is likely due to the desorption of low-molecular -weight material and volatile gases produced during the photo-oxidation following transfer of the unwashed samples to the vacuum system for analysis. However, an alternative explanation that cannot be discounted is suggested by the work of Lubarsky et al. (47) and Strobyl et al. (48), who depth-profiled the composition of UV-treated PET film and found no change in composition through the first 10 nm of the samples. Their data suggest that it is possible that although surface modification occurs through a substantial depth of material, washing only removes the top-most layers of material, leading to a very small change in the spectra after washing.

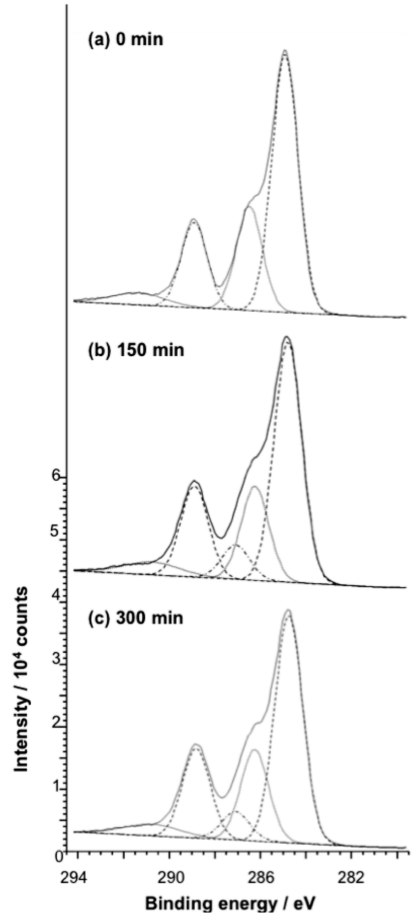

FIGURE 6. C1s spectra for PET exposed to UV light for 0 min (top), 150 min (center), and 300 min (bottom).

High-resolution C1s and O1s spectra were also acquired. The C1s spectrum of the virgin polymer exhibited three principal bonding environments (Figure 6a). A strong peak at 284.7 eV resulted from the aromatic carbon and was used as a reference. Components were additionally observed that were attributed to an ether (a peak at 286.5 eV) and an ester (at ca. 288 eV). The ester, ether, and aromatic carbon were present in a 1:1:3 ratio. In addition a small shake-up satellite was observed at 291.5 eV. The O1s spectrum exhibited two principal components, corresponding to the ether and carbonyl oxygen atoms (single and doubly bonded, respectively), with the ether component appearing at slightly higher binding energy than the carbonyl one.

Following UV exposure, the oxygen peaks broadened and they became difficult to resolve. The C1s spectra were more informative, although even here the changes were rather subtle. Figure 6 shows spectra acquired after exposures of 150, and 300 min. The most significant change in the spectrum was the appearance of a new peak, corresponding to a carbonyl carbon atom, at a chemical shift of 287 eV. A substantial increase was observed in the size of the carbonyl

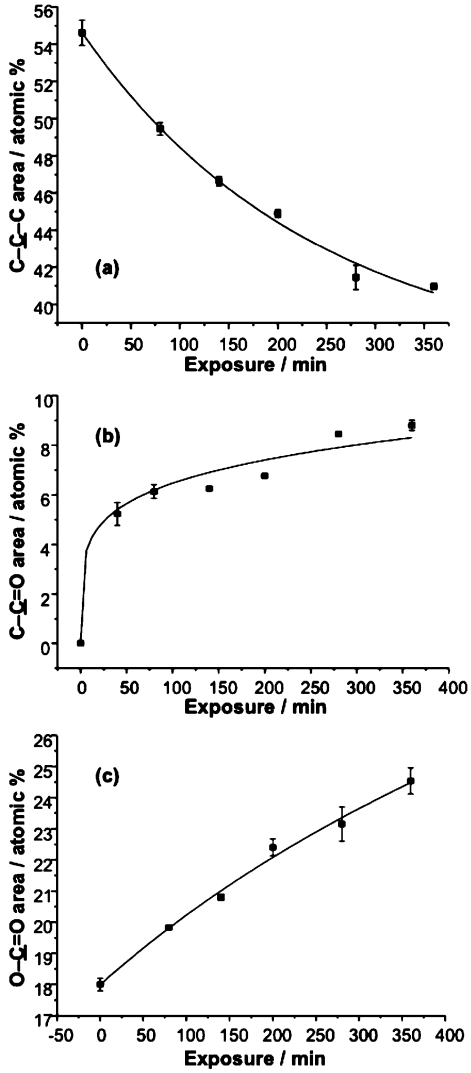

FIGURE 7. Surface composition kinetics showing the change in contributions to the C1s peak from the (a) aromatic carbon, (b) carbonyl, and (c) ester components.

component during the initial 50 min of exposure. This correlated with the contact angle data, which exhibited an initial high rate of change but then changed more slowly after 50 min.

The appearance of the new component was accompanied by a reduction in the amount of aromatic carbon from 54.6 ± 0.68 to 41.0 ± 0.15 %. The fall in the fraction of aromatic carbon (see Figure 7a) was found to be closely correlated with the fall in the total percentage of surface carbon (Figure 5). The ether contribution exhibited a negligible change from 20.5 % of the total carbon contribution at the surface. In contrast, the carbonyl component increased to reach a limiting area of ca. 8% of the total carbon signal after 6 h exposure (Figure 7b). The area of the ester component was observed to increase, to nearly 25 % of the total carbon signal (Figure 7c).

Comparison of Data from Contact Angle Measurement, FFM, and XPS. A detailed kinetic analysis proved complex because of the diversity of reaction pathways involved and because several different functional groups are modified during the photo-oxidation reaction.

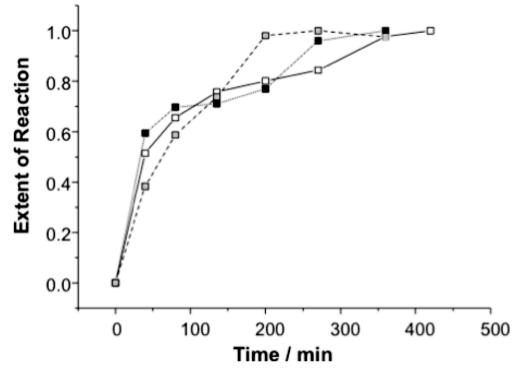

FIGURE 8. Variation in the extent of reaction, χ, as determined from contact angle (white squares), FFM (gray squares), and XPS carbonyl peak intensities (black squares), as a function of UV exposure time.

However, a simple measure of the extent of reaction may be derived from the contact angle and FFM measurements. If the final value of the cosine of the water contact angle is cos θ_f, the initial value is cos θ_i, and the value at time t is cosθ_t, then we can write, using Cassie's equation

$$\cos\theta_t = \chi\cos\theta_f + (1 - \chi)\cos\theta_i$$

where χ is the extent of completion of the reaction and $0 \leq \chi \leq 1$. Hence

$$\chi = \frac{\cos\theta_t - \cos\theta_i}{\cos\theta_f - \cos\theta_i}$$

If the FFM data are treated in the same way, an approach that is justified by the correlation between cosθ and μ shown in Figure 4, then the following equivalent expression may be derived

$$\chi = \frac{\mu_t - \mu_i}{\mu_f - \mu_i}$$

where μ_t is the friction coefficient at time t and μ_i and μ_f are the initial and final values of μ, respectively. The XPS data can also be analyzed in an analogous fashion, using the ratio of the area of each component (e.g., carbonyl or ester carbon) to the total C1s signal in place of μ or cos θ. When the data were analyzed in this way, a good correlation was found between values of χ calculated from the contact angle and FFM measurements, as expected based on the data in Figure 4. A good correlation was also observed between these sets of data and the values of χ calculated using the variation in the intensity of the carbonyl component (Figure 8). Overall, the agreement between the three approaches is excellent, emphasizing the value of FFM as a simple route to quantitative data on surface composition with high resolution. In previous studies of the plasma treatment of PET, an increase in the surface energy following treatment was found to be correlated the appearance of a carbonyl component in the C1s spectrum (49). The carbonyl groups are thought

Scheme 3. Proposed Mechanism for the Photo-oxidation of PET

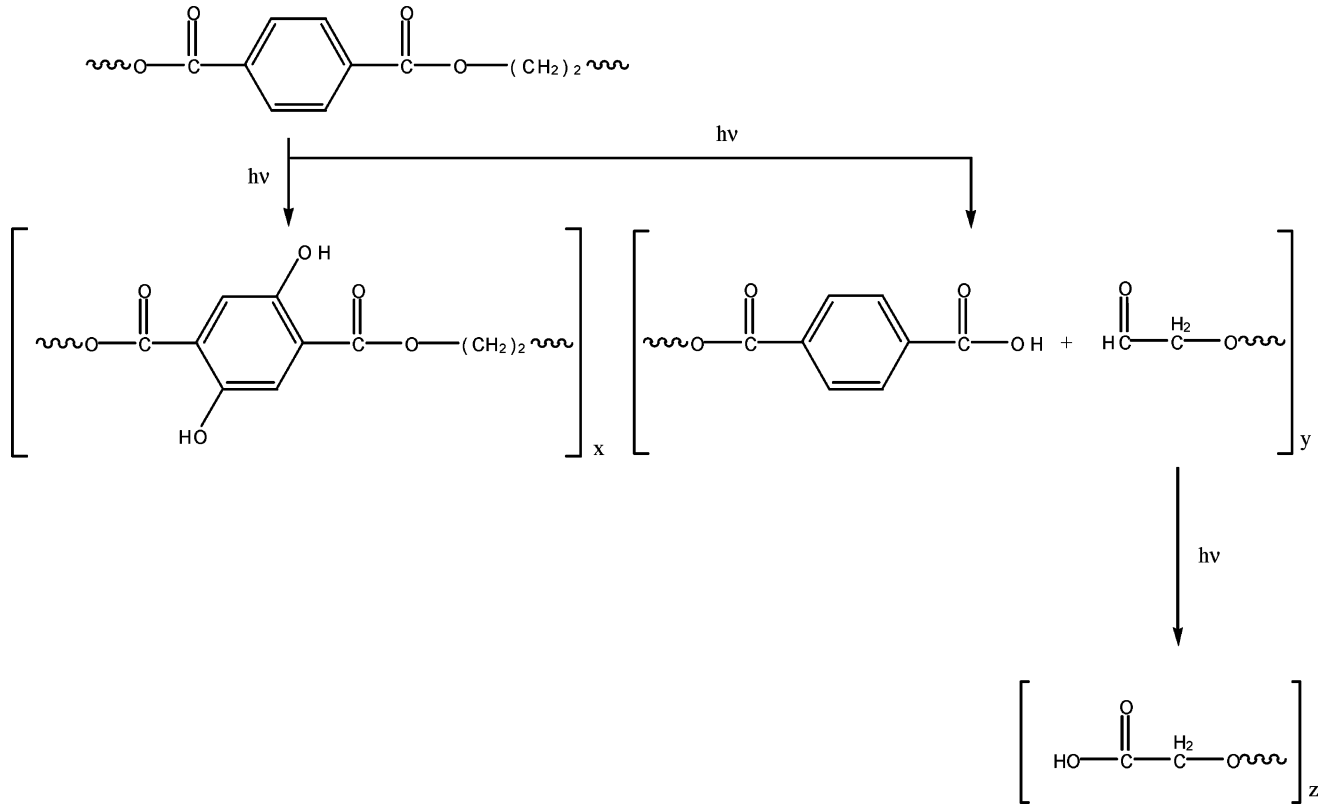

Table 1. Comparison of Observed Results with Those Predicted from the Mechanism Predicted in Reaction Scheme 3

	0	*t*	observation	inference
C−C−C	6*n*	(6 − *x*)*n*	decrease	ring hydroxylation occurs
C−C−O	2*n*	(2+ *x* − *y*)*n*	constant	rates of chain scission and ring hydroxylation are equal
O−C═O	2*n*	(2 + *z*)*n*	increase	chain scission to form aldehydes is followed by further oxidation
C−C═O	0*n*	(*y* − *z*)*n*	rate dependent	chain scission occurs, leading to aldehyde formation

to exhibit basic character and contribute to the raising of the surface free energy by increasing the acid−base component of the surface free energy.

The most significant criticism of the FFM data is that they lack the structural specificity of the XPS measurements. FFM data—at least in the present case where no effort was made, for example, to functionalize the probe—do not enable one to differentiate between, for example, contributions to the surface free energy from carboxylate and carbonyl groups. In many ways, the data are analogous to contact angle data—the chemical structural content is limited and the signal is largely determined by the surface free energy. Against this, the greater spatial resolution of FFM may be important in other circumstances, and the evidence presented here that it may yield quantitative data for complex polymer systems that correlate with macroscopic measurements is significant for polymer surface analysis at the nanometer scale.

Mechanism of Photodegradation of PET. If the mechanism of Fechine et al. is correct (29), the number of carbon atoms singly bonded to oxygen will tend to increase (XPS would not discriminate between carbon atoms bonded to ether and phenolic oxygens) and consequently there would be a decrease in aromatic carbons as one or two of these bind to the hydroxy groups to form the hydroxy substituted terephthalate, unless the rate of chain scission exceeds the rate of formation of phenolic groups. The appearance of a carbonyl species in the C1s spectrum is expected due to the formation of the aldehyde. Finally, the contribution from the ester component should remain constant. With the exception of an observed increase in the ester component, which can be explained by the further reaction of the aldehyde proposed by Grossetête et al (38), our XPS data are consistent with these findings.

Vapor-phase chemical derivatization with TFAA can derivatize hydroxyl groups selectively in the presence of carboxylic acids and carbonyl groups to a high degree (50). Fluorine peaks were observed in the survey spectrum of the fully exposed and derivatized PET, but with a very weak intensity (~0.7 %). Contact-angle data were also obtained after exposure to UV and TFAA. No significant change was observed from that of the exposed polymer. These data do not confirm the presence of the hydroxy-substituted terephthalate. However, the absence of positive confirmation does

not necessarily exclude the possibility of formation of a hydroxy-substituted ring product. First, it is thought to be a major product of the photo-oxidation because of the dramatic decrease in aromatic carbon. Second, the possibility that this derivatization would not proceed in the case of a hydroxy substituted aromatic compound must be considered because hydroxyl groups attached to aromatic rings are less strongly nucleophilic than aliphatic alcohols (on which the surface derivatization literature has largely focused). Grossetête cited the observation of an adsorption band with a maximum at 340 nm, corresponding to the fluorescent monohydroxy terephthalate, as evidence for its formation (an adsorption band for the dihydroxy substituted terephthalate was noticeably absent) (38). This degradation product was also observed in the work of Fechine et al. and Lee et al. who used UV absorbers to prevent its formation during photodegradation (29, 30). From these data it may be concluded that the main mechanism is likely to be that proposed by Fechine leading to the monohydroxy substituted terephthalate, aldehyde, and carboxylic acid. To explain the significant increase in the ester component, it is necessary to look at the work of Grossetête who reported the further oxidation of the aldehyde to form an additional carboxylic acid terminus.

Scheme 3 illustrates the proposed mechanism for the photodegradation of PET. A simple mathematical analysis can be used to predict increases and decreases in the contributions to the C1s peak. Suppose that the amount of polymer at the start of the experiment is n. The amounts of carbon atoms in the different bonding environments at time $t = 0$ will be as shown in Table 1. Suppose that a fraction x of the aromatic carbons undergoes ring hydroxylation. The amount of aromatic ring carbon atoms (with corresponding peak at 285 eV in the C1s spectrum) will decrease to $(6 - x)n$, whereas the number of carbon atoms singly bonded to oxygen will increase by the same amount. Suppose also that a fraction y of the PET follows the right-hand pathway, involving ether bond cleavage to yield a carboxylic acid and an aldehyde. The amount of C−C−O observed will decrease by yn, and the amount of C-C=O will increase by yn. Finally, if a fraction z of the resulting aldehyde groups are converted to carboxylic acids, then the amount of C−C=O will decrease by zn and the amount of carboxylate carbon will increase by the same amount. The data in Figure 7a show that the aromatic carbon component decreases by 14 at % after 350 min. Given that the change in the area of the ether peak is negligible, then $x = y$, meaning that equal proportions of the polymer molecules proceed down the alternate paths indicated in Scheme 3. If this is the case, then the total change in the areas of the carbonyl and carboxylate components (i.e., the sum of the products of the two steps shown in the right-hand pathway in Scheme 3) should also equal the change in the area of the aromatic carbon peak. The changes in the areas of the aldehyde and carboxylic acid peaks are, respectively, 8 and 7%, yielding a total of 15%, in good agreement with the change in the area of the aromatic carbon component. The fact that the intensity of the aldehyde peak approaches a steady state suggests that an equilibrium is ultimately reached in which the rate of chain scission is approximately equal to the rate of aldehyde oxidation. These data thus support the validity of Scheme 3, and suggest that ring hydroxylation and main chain scission occur with approximately equal probability.

CONCLUSIONS

The kinetics of the photodegradation of PET at the surface was observed on both the micro- and macroscale by contact angle goniometry and FFM respectively. The hydrophilicity of the surface was seen to increase as atmospheric oxygen reacted with the photosensitized polymer until it reached a limiting value after ~200 min. XPS data were then used to elucidate the mechanism of the degradation. The photodegradation process was shown to proceed through radicals formed via Norrish type I reactions, leading to a carboxylic acid and an aldehyde, in agreement with earlier work by Fechine et al. (29) and Grosstête et al. (38). There was excellent quantitative agreement between the three techniques when used to determine the extent of the reaction. The limited molecular specificity of FFM meant that for this system, XPS yielded mechanistic insights with greater precision. However, evidence was provided of the capacity of FFM to yield quantitative data on modified surfaces that correlate closely with those obtained from macroscopic surface analysis methods.

Acknowledgment. C.R.H. thanks the Engineering and Physical Sciences Research Council for a Research Studentship. The authors thank Tracie J. Whittle for assistance with the XPS measurements.

REFERENCES AND NOTES

(1) Grafstrom, S.; Neitzert, M.; Hagen, T.; Ackerman, J.; Neumann, R.; Probst, O.; Wortge, M. *Nanotechnology* **1993**, *4*, 143.
(2) Overney, R.; Meyer, E. *Mater. Res. Bull* **1993**, *18*, 26.
(3) Carpick, R. W.; Salmeron, M. *Chem. Rev.* **1997**, *97*, 1163.
(4) Kim, H. I.; Koini, T.; Lee, T. R.; Perry, S. S. *Langmuir* **1997**, *13*, 7192.
(5) McDermott, M. T.; green, J.-B. D.; Porter, M. D. *Langmuir* **1997**, *13*, 2504.
(6) Gnecco, E.; Bennewitz, R.; Gyalog, T.; Meyer, E. *J. Phys.: Condens. Matter* **2001**, *13*, R619.
(7) Xiao, X.; Hu, J.; Charych, D. H.; Salmeron, M. *Langmuir* **1996**, *12*, 23.
(8) Wei, Z.; Wang, C.; Bai, C. *Langmuir* **2001**, *17*, 3945.
(9) Flater, E. E.; Ashurst, W. R.; Carpick, R. W. *Langmuir* **2007**, *23*, 9242.
(10) Clear, S. C.; Nealey, P. F. *Langmuir* **2001**, *17*, 720.
(11) Frisbie, C. D.; Rozsnyai, L. F.; Noy, A.; Wrighton, M. S.; Lieber, C. M. *Science* **1994**, *265*, 2071.
(12) Vezenov, D. V.; Noy, A.; Rozsnyai, L. F.; Lieber, C. M. *J. Am. Chem. Soc.* **1997**, *119*, 2006.
(13) Shon, Y.-S.; Lee, S.; Colorado, R.; Perry, S. S.; Lee, T. R. *J. Am. Chem. Soc.* **2000**, *122*, 7556.
(14) Kim, H. I.; Houston, J. E. *J. Am. Chem. Soc.* **2000**, *122*, 12045.
(15) Houston, J. E.; Doelling, C. M.; Vanderlick, T. K.; Hu, Y.; Scoles, G.; Wenzl, I.; Lee, T. R. *Langmuir* **2005**, *21*, 3926.
(16) Brewer, N. J.; Leggett, G. J. *Langmuir* **2004**, *20*, 4109.
(17) Brewer, N. J.; Foster, T. T.; Leggett, G. J.; Alexander, M. R.; McAlpine, E. O. *J. Phys. Chem. B* **2004**, *108*, 4723.
(18) Major, R. C.; Kim, H. I.; Houston, J. E.; Zhu, X.-Y. *Tribol. Lett.* **2003**, *14*, 237.
(19) Brukman, M. J.; Marco, G. O.; Dunbar, T. D.; Boardman, L. D.; Carpick, R. W. *Langmuir* **2006**, *22*, 3988.

(20) Foster, T. T.; Alexander, M. R.; Leggett, G. J.; McAlpine, E. *Langmuir* **2006**, *22*, 9254.
(21) Hurley, C. R.; Leggett, G. J. *Langmuir* **2006**, *22*, 4179.
(22) Whittle, T. J.; Leggett, G. J. *Langmuir* **2009**, *25*, 2217.
(23) Chong, K. S. L.; Sun, S.; Leggett, G. J. *Langmuir* **2005**, *21*, 3903.
(24) Kumar, A. P.; Pandey, J. K.; Kumar, B.; Singh, R. P. *J. Polym. Environ.* **2006**, *14*, 203.
(25) Luzuriaga, S.; Kovářová, J.; Fortelný, I. *Polym. Degrad. Stab.* **2006**, *91*, 1226.
(26) Wegelin, M.; Canonica, S.; Alder, A. C.; Marazuela, D.; Suter, M. J.; Bucheli, T. D.; P. Haefliger, O.; Zenobi, R.; McGuigan, K. G.; Kelly, M. T.; Ibrahim, P.; Larroque, M. *J. Water Supply: Res. Technol.* **2001**, *50*, 125.
(27) Liu, R.; Schiraldi, D.; Hiltner, A.; Baer, E. *J. Polym. Sci., Part B: Polym. Phys.* **2002**, *40*, 862.
(28) Qureshi, N.; Stepanov, E.; Schiraldi, D.; Hiltner, A.; Baer, E. *J. Polym. Sci., Part B: Polym. Phys.* **2000**, *38*, 1679.
(29) Fechine, G. J. M.; Rabello, M. S.; Maior, R. M. S.; Catalani, L. H. *Polymer* **2004**, *45*, 2303.
(30) Lee, C.; Wu, C.; Lin, M. *Polym. Degrad. Stab.* **2004**, *83*, 435.
(31) Chen, R.; Meloy, J.; Daglen, B. C.; Tyler, D. R. *Organometallics* **2005**, *24*, 1495.
(32) Scott, G. *Polym. Degrad. Stab.* **1990**, *29*, 135.
(33) Wirsén, A.; Sun, H.; Albertsson, A. *Biomacromolecules* **2005**, *6*, 2697.
(34) Shiro, T. *Comprehensive Organic Synthesis*; Pergamon Press: New York, 1991.
(35) Fagerburg, D. R.; Clauberg, H. In *Modern Polyesters: Chemistry and Technology of Polyesters and Copolyesters*; Scheirs, J., Long T. E., Eds.; Wiley Blackwell: Chichester, U.K., 2003; p 626.
(36) Gotoh, K.; Kikuchi, S. *Colloid Polym. Sci.* **2005**, *283*, 1356.
(37) Laurens, P.; Petit, S.; Arefi-Khonsari, F. *Plasma Polym.* **2003**, *8*, 281.
(38) Grossetête, T.; Rivaton, A.; Gardette, J. L.; Hoyle, C. E.; Ziemer, M.; Fagerburg, D. R.; Clauberg, H. *Polymer* **2000**, *41*, 3541.
(39) Khare, A.; Deshmukh, S. *J. Plast. Film Sheeting* **2006**, *22*, 193.
(40) Day, M.; Wiles, D. M. *Can. Text. J.* **1972**, *89*, 69.
(41) Hutter, J. L.; Bechhoeffer, J. *Rev. Sci. Instrum.* **1993**, *64*, 1868.
(42) Beamson, G.; Briggs, D. *High Resolution XPS of Organic Polymers: The Scienta ESCA 300 Database*; Wiley: Chichester, UK, 1992.
(43) Beake, B. D.; Ling, J. S. G.; Leggett, G. J. *J. Mater. Chem.* **1998**, *8*, 1735.
(44) Brewer, N. J.; Beake, B. D.; Leggett, G. J. *Langmuir* **2001**, *16*, 735.
(45) Beake, B. D.; Leggett, G. J. *Phys. Chem. Chem. Phys.* **1999**, *1*, 3345.
(46) Beake, B. D.; Leggett, G. J. *Langmuir* **2000**, *16*, 735.
(47) Lubarsky, G.; Davidson, M.; Bradley, R. *Surf. Sci.* **2004**, *558*, 135.
(48) Strobyl, M.; Walzak, M.; Hill, J.; Lin, A.; Karbashewski, E.; Lyons, C. *J. Adhes. Sci. Technol.* **1995**, *9*, 365.
(49) Beake, B. D.; Ling, J. S. G.; Leggett, G. J. *J. Mater. Chem.* **1998**, *8*, 2845.
(50) Sutherland, I.; Sheng, E.; Brewis, D.; Heath, R. *J. Mater. Chem.* **1994**, *4*, 683.

AM900250Q